Univerza v Ljubljani
Fakulteta za Matematiko in Fiziko
Oddelek za Fiziko

Fizika osnovnih delcev in jedra

Gregor Kramberger

Radiation damage in silicon microstrip detectors

Postgraduate seminar

Supervisors: doc. dr. Marko Mikuž, dr. Vladimir Cindro

Ljubljana, 1996

1 Introduction

The current interest in radiation damage to semiconductor materials arises from the plans for experiments at future hadron colliders. A typical detector at the Large Hadron Collider (LHC) includes a tracking detector, which is installed in the centre of the experiment in order to record tracks of charged particles. The inner-most detector - a vertex detector is placed very close to the interaction point and locates decays of short-lived particles. Silicon detectors are best suited to meet the challenges of high accuracy and efficient track measurements, because of the high level of possible segmentation into strips or pixels.

The LHC machine will allow proton beams with energies up to 14 TeV and a luminosity of 10^{34} cm^{-2} s^{-1}. At maximum LHC luminosity 10-20 interactions occur in every beam crossing producing several hundred secondary particles. The accumulated dose over many years of high luminosity operation will be equivalent to 10^{14} neutrons cm^{-2} and 10 Mrad. The radiation causes damage to silicon bulk and surface. The surface damage seems to be manageable. It depends considerably on detector design and manufacturing, which have been well studied and understood. On the other hand the bulk damage is inevitable. It has a major influence on the leakage current and the effective doping concentration.The current causes noise, power consumption and therefore heat, and the effective doping concentration affects considerably the operational voltage. Due to the interaction of radiation and silicon atoms the periodic structure of the lattice is destroyed locally, i.e. silicon atoms are dislocated. A dislocated atom is called an interstitial atom, whereas the lattice site being empty now is called vacancy. The interstitials and vacancies form defect complexes which establish energy levels in the band gap. Most of the defect complexes contain impurity atoms e.g. carbon and oxygen. Since detector operation is foreseen to last several years the long term behaviour of these quantities is of major concern. Understanding which type of defect causes deterioration of performance is very important in our attempt to build a radiation hard detector.

In this work some basic concepts of operation of silicon microstrip detector are given in the first chapter. After that a simple microscopic view of the defects is presented together with a list of defects known so far. The third part of the seminar is dedicated to changes in detectors performance. Both, dependence on time and fluence are considered.

2 Theory and Operation of Silicon Microstrip Detectors

A silicon detector is in fact a reverse biased diode operating as an ionization chamber. Ionizing particles passing a silicon detector generate electron-hole pairs along their paths. The number of pairs is proportional to the particles' energy loss. The creation of electron-hole pair requires a mean energy of 3.6 eV. The average energy loss in silicon is about 390 eV/μm for a minimum-ionising particle. For a typical detector thickness of about 300 μm, one obtains $3 \cdot 10^4$ electron-hole pairs in average, a signal detectable with low-noise electronics.

However, pure (intrinsic) silicon is not appropriate for operation as a detector, since the background originating from thermally excited $e-h$ pairs is too large. In pure silicon concentrations of electrons (n) and holes (p) are equal $n = p = n_i$ and can be calculated from

$$n\,p \;=\; n_i^2 = N_C\,N_V\,\exp(\frac{-E_g}{k_B T}) \tag{1}$$

where N_c ($= 2.8 \cdot 10^{19}$ cm^{-3} at 300 K) and N_v ($= 1.04 \cdot 10^{19}$ cm^{-3}) are effective densities of states at the conduction and valence band edges, respectively, E_g=1.12 eV is the band gap, k_B the Boltzmann constant and T the temperature. At room temperature the intrinsic carrier density is $n_i \equiv n = p = 1.5 \cdot 10^{16}$ m^{-3}, which gives for a detector of 1 cm^2 surface and a thickness of 300 μm $5 \cdot 10^8$ for the total number of free current carriers. [†] The fluctuation of this value represents the background which is of the same order as the expected signal. The concentration of free current carriers could be reduced by cooling the detector, which is not a very practical way.

2.1 $P - N$ junction

The number of electrons and holes in silicon can be changed significantly by doping it with donors and acceptors. Donors are atoms which have in addition to the four electrons, needed for the covalent bond, one electron they donate to the conduction band. Hence the number of electrons in the conduction band at room temperature equals the number of donors. Acceptors are atoms having one electron missing to form bondings to all neighbours. To complete the missing bond they accept an electron from the valence band, where a hole is left. Thus, also the number of holes equals the number of acceptors. However, in every silicon the relation $n_i^2 = n\,p$ holds. If the concentration of donors N_D exceeds the concentration of acceptors N_A ($N_D > N_A$) the material is called n-type, where electrons are majority carriers and holes minority carriers. Otherwise ($N_A > N_D$) the material is called p-type, holes are majority carriers and electrons minority carriers.

[†] It is impossible to make pure silicon, therefore the background is even larger.

Very often phosphorus is used as a donor, and boron as an accceptor. The energy level of the remaining phosphorus electron in silicon is very close (ΔE_C=0.044 eV) to the conduction band and thus even at very low temperature all phosphorus atoms are ionised ($N_D \approx n$). On the other hand the energy level of the boron atom is very close (ΔE_V=0.046 eV) to the valence band. Hence, all the boron levels are occupied by valence electrons, leaving the corresponding concentration of holes in the valence band ($N_A \approx p$).

When the doping concentration changes abruptly from a surplus of acceptors N_A on the p-side to a surplus of donors N_D on the n-side an abrupt junction, the $p-n$ junction, is obtained (figure 1). At the junction a gradient of electron and hole densities appears resulting in a diffusive migration of majority carriers across the junction. This migration leaves the left-hand region with a net negative charge and the right-hand region with a net positive charge, the so called space charge (SCR) or depletion region. This space charge is due to unneutralised, immobile acceptor and donor ions. One should note that in the space charge region there are almost no free carriers. The initial migration of carriers

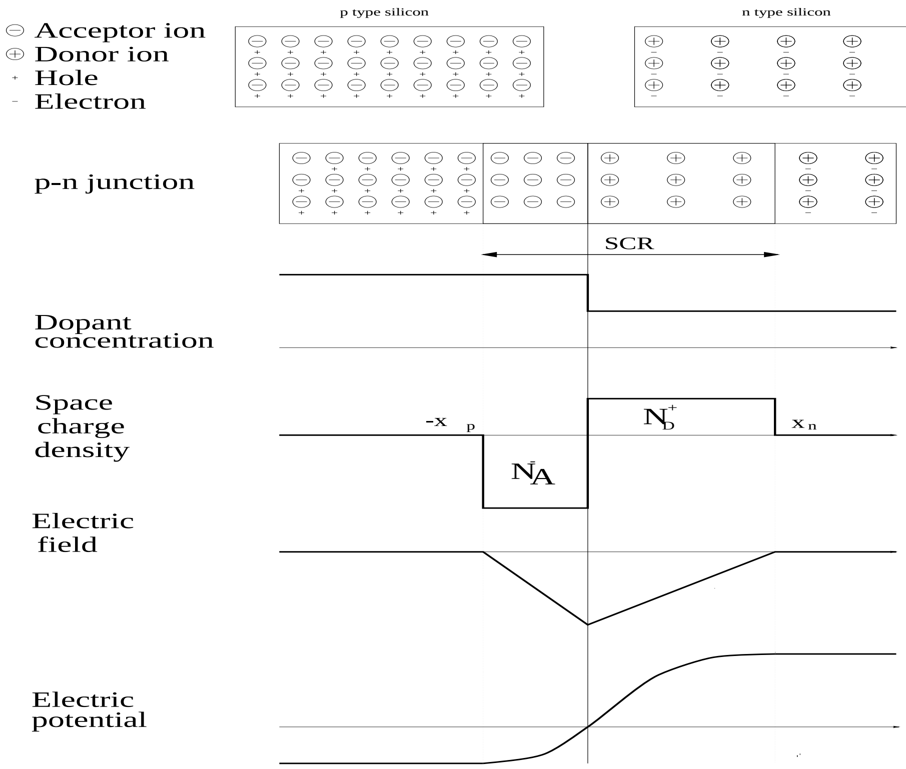

Figure 1: The $p-n$ junction: dopant concentration, space charge density, electric field strength and electric potential.

across the junction sets up a electric potential barrier to prevent further migration. Since the requirement for equilibrium in this system is that there is no net steady-state flow across the junction, the barrier is self adjusted - the Fermi level has to be constant trough the junction. Hence the conduction band and the valance band are bent (figure 2). The electric properties of the junction can be calculated from Poisson's equation.

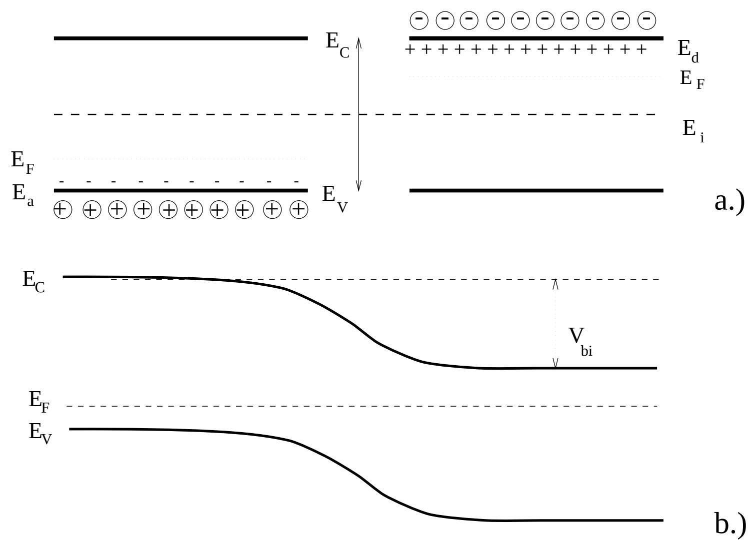

Figure 2: a.) Energy diagram for n-type (left) and p-type (right) silicon. E_D denotes the energy level of the donor and E_a that of the acceptor. b.) Energy diagram of $p-n$ junction, V_{bi} represents built in potential.

Results for electric potential and electric field are shown in figure 1. It can be seen that the width of depleted region on each side of the junction is inversely proportional to dopation. The potential difference between the bottom of the conduction band on the p-side and its bottom on the n-side is the built-in potential V_{bi} (figure 2). Im most practical cases the doping of one of the regions by far exceeds that of the other, therefore $N_1 \gg N_2 \to x_1 \ll x_1 \approx d$ the thickness of depleted region. V_{bi} can be calculated from

$$V_{bi} = \frac{e_0 \, N_D \, d^2}{2\epsilon_S}. \tag{2}$$

expressing the thickness of the depleted region

$$d = \sqrt{\frac{2\,\epsilon_S}{e_0\,N_D}\,V_{bi}} \tag{3}$$

Because in high resistivity n-type material ($\rho > 2$ kΩcm) donor and acceptor concentrations are of the same order of magnitude, N_D has to be replaced by the difference of the donor and acceptor concentrations $N_{eff} = |N_D - N_A|$.

For charged particle detection, the $e-h$ pairs created in the depletion region by a traversing particle are separated by the electric field, collected and read out. The charge created in the neutral, non-depleted region recombines with free carriers and is lost.

Increasing the width of the space charge region increases the collected signal. Ideally one would like to have the whole thickness depleted of free carriers.

It is possible to increase the width of the SCR by applying an external potential difference, V, typically of the order of hundred volts and of the same sign as V_{bi}. The junction is reverse biased.

$$d(V) = \sqrt{\frac{2\,\epsilon_S}{e_0\,N_{eff}}\,(V_{bi}+V)} = \sqrt{\frac{2\,\epsilon_S}{e_0\,N_{eff}}\,V} \tag{4}$$

At certain voltage $V = V_{fd}$ the detector is fully depleted, meaning $d = D$, where D is the detector thickness

$$V_{fd} = \frac{e_0 N_{eff} D^2}{2\,\epsilon_S} \quad \text{and} \quad N_{eff} = \frac{2\,\epsilon_S}{e_0}\,\frac{V_{fd}}{D^2} \quad . \tag{5}$$

In order to make a silicon detector position sensitive, the heavily doped side is divided into narrow strips. One coordinate of particle transition is then given by the the strip number. Figure 3 shows schematically the cross section of a silicon microstrip particle

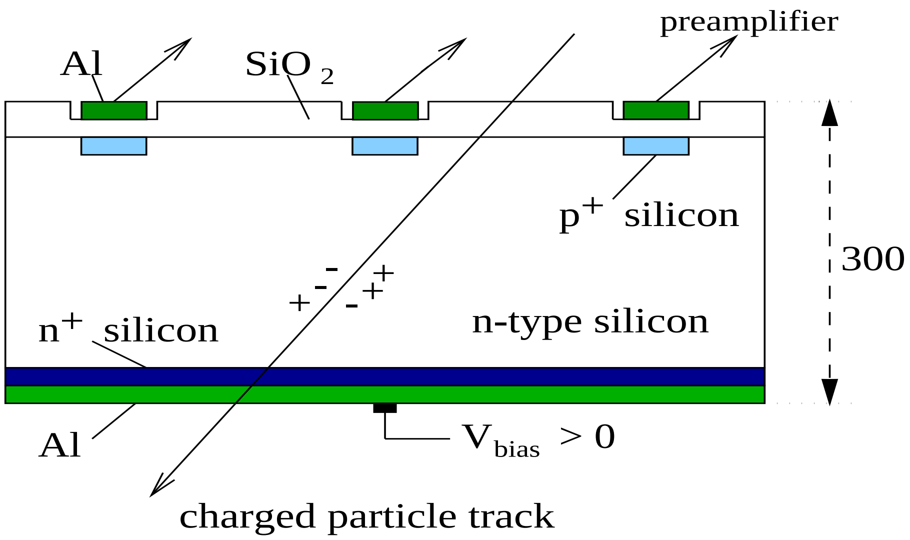

Figure 3: Schematic view of AC- coupled p^+n (p strips, n bulk) type detector. Dimensions are in μm.

detector. Additionally to n silicon there is p^+ silicon [‡] on one side and a layer of highly doped n^+ on the other. Such a detector is called p^+n detector, where holes are collected at the p^+ strips. The p^+ strips serve to polarise the junction, and the n^+ layer to prevent the depletion zone from reaching the back plane and to ensure a good ohmic contact. Strips (p^+) must be metallized to allow ultrasonic bonding of strips to the electronics. This can

[‡] Plus over p means heavily doped.

be done in two ways, either aluminium is in contact with p^+ strips (DC - coupling) or a thin layer of isolator is squeezed between them (AC -coupling).

Also possible are n^+n (n-strips, n-bulk) detectors, where p^+ and n^+ layers exchange roles. Instead of holes as it is the case in p^+n detectors, electrons are collected. Due to higher mobility of electrons the charge collection time is shorter. The SCR starts to grow from the rear side of the n^+n detector, since the $p^+ - n$ junction is formed at the backplane. Such a detector has to be operated fully depleted.

2.2 Detector Performance

The created charge, signal, is collected by a charge-sensitive preampflifier. This, together with the detector, introduces noise. The noise of the system can be described by the following equation

$$N^2 = KI_{rev}\tau + \frac{LC^2}{\tau} + M \tag{6}$$

where K, L, M are parameters depending on the system, τ is the shaping time constant, and I_{rev} and C are the reverse current and the total capacitance on the input of the preamplifier, respectively. It is obvious that both reverse current and capacitance should be as small as possible. Both, I_{ref} and C change due to irradiation and influence detector performance.

When a diode is reverse biased, only a small current, called leakage current or reverse current I_{rev} flows. It can be divided into two parts: the bulk generation current I_{BGC} and the surface current I_{SC}. If no bias is applied $e - h$ pairs are generated and annihilated continuously and no net current flows. However, due to the reverse bias applied, the recombination is suppressed and therefore a reverse current occurs. The generation can be greatly increased by energy levels in the centre of the band gap and is strongly temperature dependent. Those levels are mainly caused by impurities and dislocations in the bulk. Because only the centres which are in the depletion region (SCR) contribute to the bulk generation current, I_{BGC} depends on the voltage in the same way as the width of the SCR.

$$I_{BGC} \propto \sqrt{V} \tag{7}$$

It saturates when the applied voltage exceeds the depletion voltage.

Surface currents have many causes, which are not fully understood. In case of proper fabrication and handling the surface currents are negligible, but due to mechanical damage, humidity or other contamination of detector surface, they can contribute significantly to the leakage current.

The capacitance of the detector can be calculated from

$$C = \frac{dQ}{dV} = \frac{dQ}{d(d)}\frac{d(d)}{dV} \tag{8}$$

The space charge of SCR with a depth d is $Q = e_0 N_{eff} A d$, where A is the detector surface. Using (4) one gets

$$C = A\sqrt{\frac{\epsilon_S\, e_0\, N_{eff}}{2V}} = \epsilon_S \frac{A}{d}. \tag{9}$$

Of course the width SCR is limited by the thickness D of the detector and equation (4) is valid only for $d \leq D$. At $V > V_{fd}$ the capacitance remains constant, because the SCR can not be thicker than the detector itself.

In order collect all $e - h$ pairs and get the highest signal the detector has to operate at $V \geq V_{fd}$. As it will be shown latter, some over-bias is necessary to collect all pairs produced by particles. The ratio between collected charge and noise the signal to noise ratio, should be as high as possible.

3 Surface and Bulk Damage

Damage caused by radiation can be divided into two groups, surface damage and bulk damage. Surface damage seems to be better understood and can be controlled by the design and manufacturing process.

Surface related effects that have been observed depend on the design and manufacturing process, so general conclusions are difficult to draw. Charge accumulation at the silicon-oxide interface significantly decreases the inter-strip resistance on the junction side of the of microstrip detectors. Therefore the charge has to be collected very quickly to minimise the loss due to leakage to neighbouring strips. To avoid breakdown problems through silicon oxide the use of silicon nitride is suggested.

Further discussion will be limited to bulk damage, which dominates detector properties after irradiation.

3.1 Defect Generation

The principal cause of bulk damage is the interaction of incoming particles and the lattice atoms either by a collision triggering a displacement or by a nuclear reaction. Reactions, relevant for direct defect generation are those resulting in a nucleus of a different atomic number. The product of such a reaction is an impurity atom, which may influence the electrical properties of the silicon. However the damage by nuclear reactions is dominated by energy release of excited nuclei.

A lattice atom, displaced by an incoming atom, is termed as the primary knock-on atom (PKA) which may then take up an interstitial position in the lattice. The former site of the dislocated atom is known as a vacancy. A pair of vacancy and dislodged atom is called the Frenkel defect or close pair. An average energy E_d of about 25 eV is required to dislocate PKA. If more energy is transfered the PKA will lose the surplus of energy by ionization or by causing further displacements which may proceed in a cascade manner. The maximum energy which can be transfered from an incoming particle of mass m_x and energy E_x to the silicon atom can be deduced from the kinematics of the collision

$$E_{max} = 4E_x \frac{m_x m_{Si}}{(m_x + m_{Si})^2} \tag{10}$$

As opposed to charged particles which prefer transfer of only small energies, for neutrons all energy transfers in the entire range between E_d in E_{max} are of similar probability. The slowed down atoms are likely to release the remaining kinetic energy in a very short range causing a disordered region. At least 5 keV are necessary to form a disordered region which is also known as a damgage cluster.

Usually the damage caused by radiation is measured as a function of dose, which is defined as the absorbed energy per unit mass (1 Gy=1 J/ kg). But the total energy released by a particle in the semiconductor is not an adequate measure, because the energy

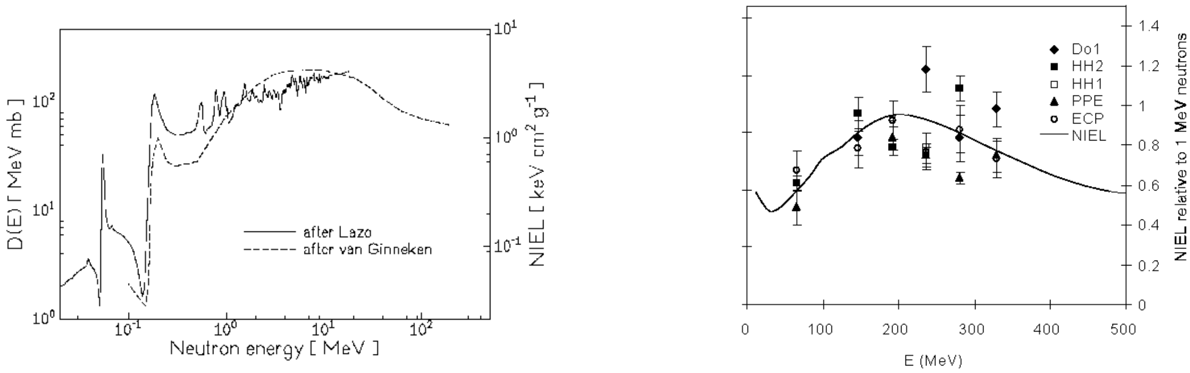

Figure 4: a.) The calculated damage function and the non-ionising energy loss (NIEL). b.) Measured and calculated values for pion non-ionising energy loss normalised to 1 MeV neutrons.

loss due to ionization is a reversible process and causes no durable damage. The generated electron-hole pairs in silicon recombine. The damage in silicon is only a function of the non-ionising energy loss (NIEL) and it is independent of particle type [§] for the same NEIL. The NIEL in turn scales linearly with the displacement damage cross section, which is also called the damage function ($D(E_x)$). The ratio between ionizing energy loss and non-ionizing energy loss is very large, i.e for 500 MeV pions

$$\frac{-dE/dx(500\mathrm{MeV}\ \pi^{\pm})_{ionizing}}{-dE/dx(500\mathrm{MeV}\ \pi^{\pm})_{non-ionizing}} \approx \frac{1.6\mathrm{MeV\,g^{-1}\,cm^{-2}}}{1.2\mathrm{keV\,g^{-1}\,cm^{-2}}} = 1400 \quad .$$

The damage caused by different particles is usually compared with the damage caused by neutrons. Since D depends on neutron energy (figure 4), the damage done by 1 MeV neutrons is taken as a reference point. In order to allow universal comparison of results it is common practice to refer to the equivalent fluence Φ_{eq} of 1 MeV neutrons which would have caused the same damage as the fluence Φ of particles really applied. Φ is converted into Φ_{eq} by multiplying it with so called hardness factor κ (table 1).

$$\Phi_{eq} \; = \; \kappa\,(\mathrm{spectrum,\ particle\ type})\,\Phi \tag{11}$$

The standard value of the damage cross section at $E_{neutron} = 1$ MeV is $D(1\ \mathrm{MeV}) = 95$ MeV mb.

As it was mentioned there are two classes of defects; Frenkel pairs and clusters. The generation rates (concentration n_d per unit fluence) are

$$g \; = \; \frac{n_d}{\Phi_{eq}} = \begin{cases} 0.33\ \mathrm{cm}^{-1} & \text{clusters} \\ 2.09\ \mathrm{cm}^{-1} & \text{Frenkel pairs} \end{cases} \tag{12}$$

[§]This has been shown for protons, neutrons and pions.

Particle	Energy (mono-energetic)	Hardness factor κ
Neutron	1 MeV	1
Proton	24 GeV (CERN PS)	0.93
Pion	236 MeV (PSI πE1)	0.93

Table 1: Hardness factor for different particle types.

where $g_{Frenkel}$ excludes the part of pairs, which recombine immediately. Both constituents of Frenkel-defects, the interstitial atom (I) and the vacancy (V) are highly mobile for temperatures above 4 K (I), respectively 150 K (V). Migrating through the crystal they form defect complexes, either with impurity atoms, particularly oxygen (O) and carbon (C), or themselves. Reaction rates are controlled by the concentration of impurities and defects and their relative capture radius. The most relevant defect configurations are shown schematically in figure 5. There are two groups of reactions. Group A reactions are

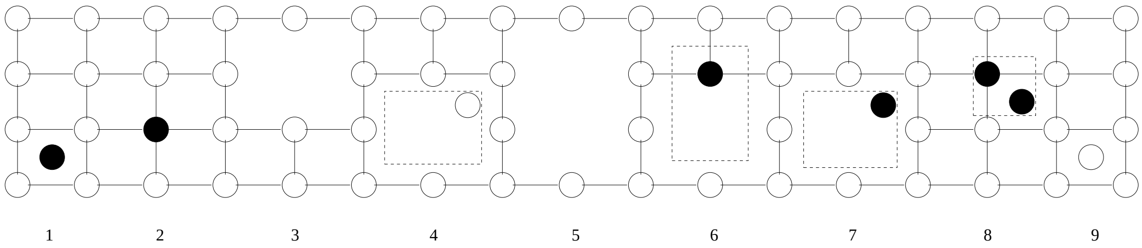

Figure 5: Various possible defect configurations: 1.) interstitial impurity atom, 2.) substitutional impurity atom (phosphorus as donor), 3.) vacancy (V), 4.) close pair, 5.) divacancy (V-V), 6.) substitutional impurity atom and vacancy (VP complex), 7.) interstitial impurity atom and vacancy (VO complex), 8.) impurity atoms on substitutional and interstitial lattice position (C_s-C_i complex), and 9.) interstitial silicon atom. The indexes $_i$ and $_s$ stand for interstitial and substitutional.

for vacancies and interstitials diffusing throughout the crystal. The group B reactions only have a significant chance of occurring during a PKA cascade, since pairing of vacancies generated in distances greater than 50 nm is insignificant.

There are four dominant vacancy related defect complexes: VO and V_2O, VP and V_2, which are stable at room temperature. Beside that, the vacancy can be also captured by impurity atoms other than oxygen and carbon, but these formations are not stable.

The interstitial atoms contribute to complex formation mainly by replacing other atoms and recombining with vacancy related defects. Replacement of impurity atoms gives rise to the formation of further defect complexes (table 2).

The physical properties of clusters are not determined yet, only theoretical models have been proposed. In the first phase the disordered region consists of many Frenkel defects. Due to their high mobility, silicon interstitials diffuse rather quickly and leave

Primary Vacancies	Primary Interstitials	Replaced impurities
Group A		
V + P $\rightarrow$ VP V + O $\rightarrow$ V O V + VO $\rightarrow$ V_2O V + C_i $\rightarrow$ C_s V + V_2O $\rightarrow$ V_3O V_2 + V $\rightarrow$ V_3	I + VP $\rightarrow$ P I + VO $\rightarrow$ O I + V_2 $\rightarrow$ V I + C_s $\rightarrow$ C_i I + V_3O $\rightarrow$ V_2O	C_i + C_s $\rightarrow$ C_i-C_s C_i + O_i $\rightarrow$ C_i-O_i C_i + P_s $\rightarrow$ C_i-P_s
Group B		
V + V $\rightarrow$ V_2 V_2 + V $\rightarrow$ V_3	I + V $\rightarrow$ S_i	

Table 2: Survey of possible defect reactions. Group A reactions are caused by diffusion of interstitials and vacancies throughout the crystal. To Group B belong the reactions, which have a significant chance of occurring during a PKA cascade.

behind the corresponding vacancies which are less mobile. The remaining vacancies are assumed to combine to vacancy complexes such as V_2 or V_3. On the other hand, the interstitial atoms are supposed to replace substitutional impurity atoms in the vicinity of the highly damaged region. The impurity atoms in turn form defect complexes. Thus the final and stable state of the cluster consists of a core of vacancy complexes with a radius $r_1 = 10$ nm and a shell of defects complexes with a radius $r_2 = 100$ nm. Due to the high defect density the band structure is locally disturbed (figure 6).

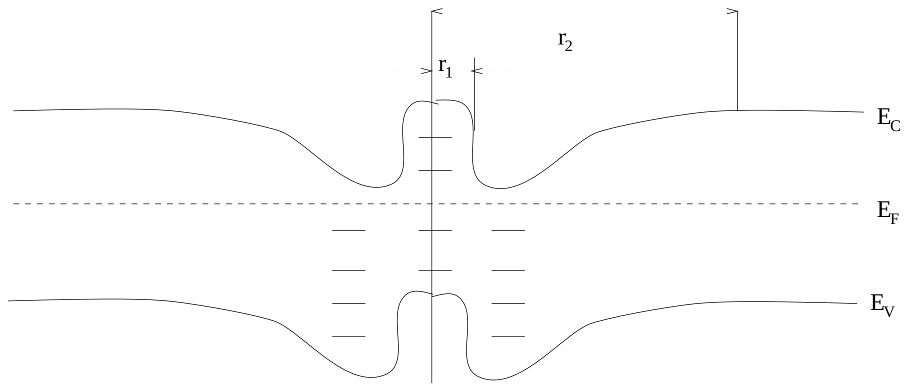

Figure 6: Local disturbance of band structure caused by a cluster.

4 Properties of Deep Energy Levels

As mentioned, particles traversing detector distort the lattice. As a consequence, each of the defects in table 2 introduces an energy level in the band gap. The occupation of an energy level E_T in the band gap can be described as a statistical process. Four competitive ways are possible to change its occupation (figure 7).

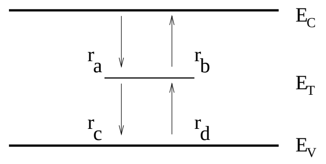

Figure 7: Emission and capture processes of an energy level E_T. Arrows present electron transitions.

- electron capture from the conduction band : $r_a = c_n \, n \, p_T$
- electron emission to the conduction band : $r_b = e_n \, n_T$
- hole capture from the valence band : $r_c = c_p \, p \, n_T$
  (equivalent to electron emission to the valence band)
- hole emission to the valence band : $r_d = c_p \, p_T$
  (equivalent to electron capture from the valence band)

where $r_{a,b,c,d}$ are emission and capture rates respectively, $c_{n,p}$ capture coefficients for electrons and holes, $e_{n,p}$ their emission probabilities, n, p concentration of free electrons and holes, n_T concentration of occupied levels and p_T concentration of non-occupied levels. The total trap concentration yields

$$N_T = n_T + p_T \quad . \tag{13}$$

The capture coefficients are products of the capture cross section $\sigma_{n,p}$ and the thermal velocity $v_{n,p}$ for electrons and holes respectively:

$$c_n = \sigma_n \, v_n \quad , \quad c_p = \sigma_p v_p \tag{14}$$

Emission probabilities are given by

$$e_n = \sigma_n v_n N_C e^{-(E_C - E_T)/k_B T} \quad , \quad e_p = \sigma_p v_p N_V e^{-(E_T - E_V)/k_B T} \quad . \tag{15}$$

Assuming $N_c \approx N_v$, emission probabilities in thermal equilibrium can be expressed in terms of the intrinsic carrier density n_i (1) as follows

$$e_n = \sigma_n v_n n_i e^{(E_T - E_i)/k_B T} \quad , \quad e_p = \sigma_p v_p n_i e^{(E_i - E_T)/k_B T} \quad , \tag{16}$$

where $E_i \approx (E_V + E_C)/2$. As expected, the rate for emission of electrons is higher if the trap is closer to the top of the conduction band and vice versa for holes.

The change in concentration of occupied traps per time is the sum of four competitive processes

$$\frac{dn_T}{dt} = r_a - r_b - r_c + r_d \qquad (17)$$

For the SCR it is assumed that no free charge carriers exist ($n = p = 0$). Thus no capture will occur and upper equation is reduced to

$$\frac{dn_T}{dt} = -r_b + r_d \qquad (18)$$

Using equation (13) it follows

$$\frac{dn_T}{dt} = e_p N_T - (e_p + e_n) n_T \qquad (19)$$

For a steady state $\frac{dn_T}{dt} = 0$, hence the fraction of occupied traps f_T is given by

$$f_T = \frac{n_T}{N_T} = \frac{e_p}{e_p + e_n} \qquad (20)$$

Since the junction is no longer in thermal equilibrium, the Fermi level does not describe the probability of occupancy. To determine the charge of the trap (charge state) with energy E_T in SCR a third energy level, associated with the properties of the level E_T, is introduced.

$$E_1 = E_i + \frac{k_B T}{2} \ln\left(\frac{\sigma_p}{\sigma_n}\right) \qquad (21)$$

with E_i being the intrinsic Fermi-level and σ_n and σ_p cross sections of the trap for electrons and holes. In the SCR E_1 replaces the Fermi level. Equation (20) can be rewritten

$$f_T = \frac{n_T}{N_T} = \frac{1}{1 + \exp\left(\frac{2(E_T - E_1(T))}{k_B T}\right)} \qquad (22)$$

As can be seen, f_T depends exponentially on temperature. Therefore energy levels in SCR are almost empty if $E_T > E_1$ and almost filled if $E_T < E_1$. Donor like states will be neutral in the lower half of the band-gap, because they are filled , whereas acceptor-like states will be neutral in the upper half and negatively charged in the lower half of the gap (figure 8). Thus donor-like states contribute to the space charge only when they are in the upper half and acceptor-like states only in the lower half of the energy gap. The contribution of energy levels close to mid-gap is governed by the temperature (figure 9).

For some of the most important complexes in table 2 the energy levels and charge states are shown in figure 10.

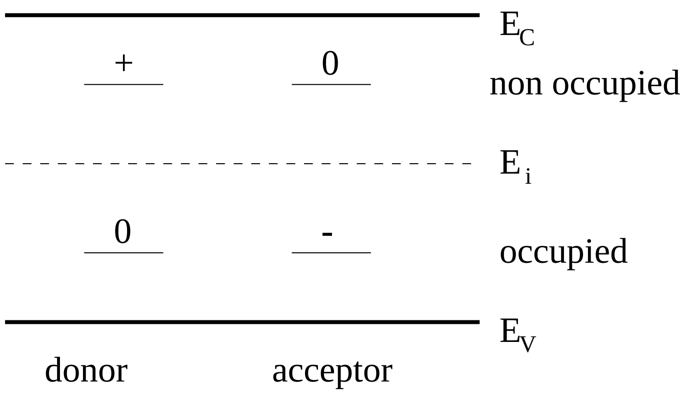

Figure 8: Charge state of donors and acceptors in the SCR.

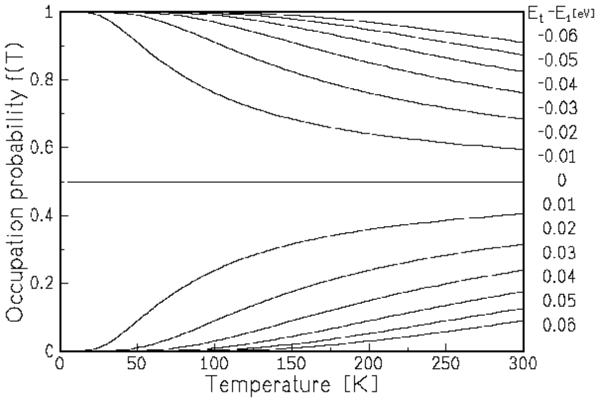

Figure 9: Occupation probability of a mid-gap energy level in the SCR ($\sigma_n/\sigma_p = 1$).

4.1 Time evolution of Defects - Annealing

After the short term reactions are completed, a state close to equilibrium is reached. However some of the generated defects are not stable in long-time terms but due to vibrational energy from the lattice they are mobile or likely to dissociate. For the dissociation a certain energy E_d is needed to overcome the binding energy of the complex. Both constituents are free then and may migrate as a single defects through the crystal. Two possibilities have to be taken into account:

- the defect is migrating to a surface or an interface which acts like a sink
- the defect reacts with another defect and forms a new defect complex

A migration energy E_m is needed for the jump from one lattice site to the neighbour one. For a reaction with another defect, a reaction energy E_r is required. Typical values of E_d, E_m, E_r are in the eV-range.

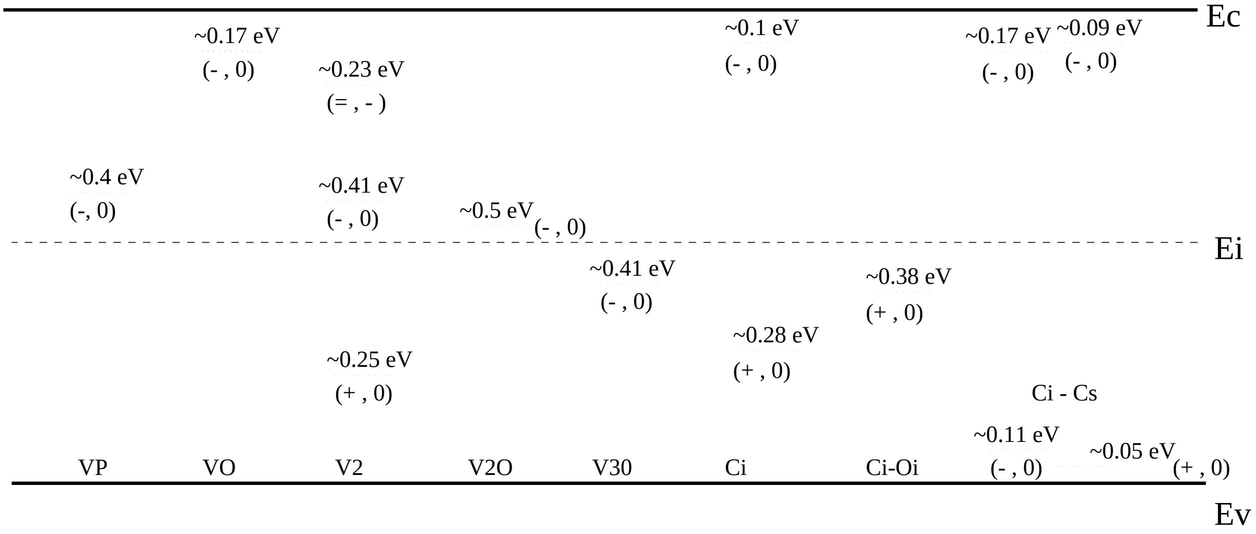

Figure 10: Energy levels of vacancy and carbon related defects (except C_i-P_s). The change of charge state is shown in brackets, e.g. minus to neutral (-,0). Above the line the energy of the trap is written; in the lower half ΔE_V and in the upper band ΔE_C. Sign = means the double charged state.

Since the energy has to be supplied by lattice vibration, the rate $\hat{k}$ at which lattice jumps (migration), dissociations or reactions occur is governed by the temperature T. The $\hat{k}$ is given by: ¶

$$\hat{k} = \hat{k_0} \exp(\frac{-E_{d,m,r}}{k_B T}) \quad , \tag{23}$$

where $\hat{k_0}$ is the frequency factor, which can be associated with the most abundant phonon frequency of about 10^{13} s^{-1} at room temperature ($\hat{k_0} = k_B T/h$).

Thus the stability or mobility of a defect depends on crystal temperature. Moreover the reaction probability of two defects, the dissociation of a complex as well as the ability of the defect to migrate can be effected by the charge state. And the charge state in turn is in many cases a question of temperature as well, because it depends on the Fermi-level, which moves with temperature.

The dissociation of the defects can be easily described as a process of first order ‖

$$-\frac{dN_X}{dt} = \hat{k} N_X \quad , \tag{24}$$

¶At typical energies $E_{d,m,r}$ this is the tail of Bose-Einstein distribution.

‖The rate of dissociation of defects is proportional to their number.

where N_X is the concentration of a defect X, which decays with the reaction constant $\hat{k}$. Solving equation (24), the time dependence N_X is found to be:

$$N_X(t) \;=\; N_{X,0}\exp(-\hat{k}(t-t_0)) \quad , \tag{25}$$

where $N_{X,0}$ is the concentration of X at time t_0. In the case of two homogeneously distributed defects X_1 and X_2, which combine to a defect complex $Y(X_1+X_2 \rightarrow Y)$ the rate equation is given by:

$$-\frac{dN_{X_1}}{dt} \;=\; -\frac{dN_{X_2}}{dt} \;=\; \tilde{k}N_{X_1}N_{X_2} \quad , \tag{26}$$

if the reaction of X_1 and X_2 is diffusion limited ($E_m > E_r$). Assuming both defects react as soon as their distance is smaller than $r_{1,2}$ the reaction constant $\tilde{k}$ can be written as:

$$\tilde{k} = 4\pi D\, r_{1,2} \quad . \tag{27}$$

The diffusion constant D is proportional to geometrical lattice quantities and proportional to $\hat{k}$ as well. Therefore D has the same temperature dependence as given in (23). The geometrical lattice quantities can be summarised into a distance R which scales with atomic distances:

$$\tilde{k} \;=\; R^3\,\hat{k}_0\exp(\frac{-E_m}{k_BT}) \quad . \tag{28}$$

R may be enlarged due to attractive Coulomb forces. From (28) becomes evident that $\tilde{k}$ is a quantity of volume per unit time, while $\hat{k}$ gives the rate of decaying complexes per unit time.

If both X_1 and X_2 are not present in similar concentration i.e. $N_{X_1} \gg N_{X_2}$ the solution of (26) is (25) with $\hat{k} = \tilde{k}N_{X_1}$. In that way only the case of $N_{X_1,0} \approx N_{X_2,0}$, which is exact for $X_1 = X_2$, is considered for the second order process. For simplicity throughout the following $N_{X_1} = N_{X_2} \equiv N_X$ will be used. The equation (26) can then be rewritten

$$-\frac{dN_X}{dt} \;=\; \tilde{k}N_X^2 \quad . \tag{29}$$

The resulting density $N_Y(t)$ is given by

$$N_Y(t) = N_{X,0}\left(\frac{1}{1+\tilde{k}N_{X,0}(t-t_0)}\right) \quad . \tag{30}$$

where $N_{X,0}$ is the concentration at time $t = t_0$.

The main difference between first and second order equation is that in (30) the reaction speed depends on the concentration $N_{X,0}$, while the time dependence in (25) is determined only by the reaction constant $\hat{k}$. For comparison the half life periods ($t_{1/2} : N_X(t_{1/2}) = 1/2N_{X,0}$) in the first or second order case are given in (31).

$$t_{1/2} = \frac{\ln 2}{\hat{k}} \quad , \quad t_{1/2} = \frac{1}{N_{X,0}\tilde{k}} \quad . \tag{31}$$

5 Changes in Detector Performance

Due to irradiation induced defect levels the detector performance is deteriorated in three different ways.

- The effective space charge is changed by defects which are charged in the SCR. Hence the depletion voltage changes, and the operational voltage may be affected.
- The current generated in the SCR increases mainly due to energy levels in the middle of the band gap as it will be shown later. Current is a source of noise to the detector system, and moreover it will lead to considerable power consumption and heat the system.
- The charge collection deteriorates, because charge carriers are trapped in energy levels located in the band gap. This leads to an error in energy calibration and a smaller signal to noise ratio.

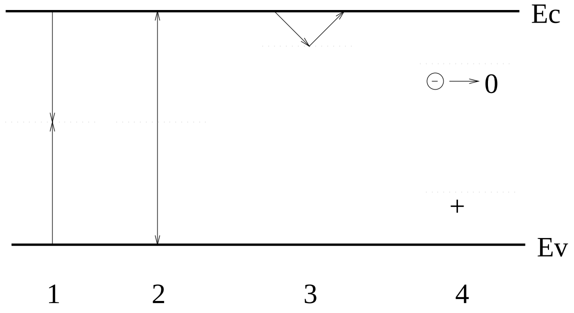

Figure 11: Effects on detector properties. 1. recombination, 2. generation, 3. trapping and detrapping and 4. compensation.

5.1 Effective Doping Concentration

The space charge changes due to trap levels which are charged in the SCR. As already shown in figure 8, non-occupied donor levels in the upper half of the band gap and occupied acceptor levels in the lower half are charged. Thus irradiation-induced generation of acceptors levels in the lower half can change the sign of space charge from positive to negative.The space charge also changes due to donor or acceptor removal, that is, the corresponding atoms are combined with vacancies or impurity atoms and lose their ability to donate or accept electrons.

Trap levels close to the middle of the energy gap also, contribute to the space charge. A certain fraction f_T is occupied by electrons and hence contributes negative charge if the trap is of acceptor type. If otherwise the trap is of donor type the non-occupied traps will contribute positive charge.

Summarising the possibilities to change the effective space charge concentration, the expression given in equation (2.1), assuming only shallow doping levels, has to be extended:

$$N_{eff} = |N_D^s - N_A^s + N_D^{ds} - N_A^{ds} + (1 - f_T)N_D^m - f_T N_A^m| \tag{32}$$

where s denotes shallow, ds deeper shallow, and m mid-gap - deep levels of which the fraction f_T is occupied.

The neutron fluence dependence of the effective doping concentration N_{eff} as determined from the depletion voltage V_{fd} (equation (5)) is shown in figure 12. For low fluences

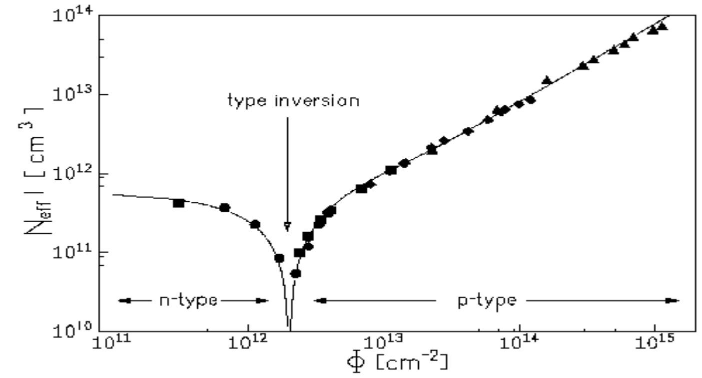

Figure 12: Effective doping concentration as function of fluence after correction for self annealing. The solid line is a fit according to (33).

a non-linear decrease of N_{eff} is observed which is assumed to be due to donor-removal. Those phosphorus atoms which combine with vacancies to form VP centres do not contribute to donor concentration anymore. Acceptor removal is assumed to be negligible, because the corresponding defect, VB centre, anneals out very rapidly at room temperature. At $\Phi \approx 5 \cdot 10^{12}$ cm^{-2}, N_{eff} ** drops close to zero and then increases linearly with fluence. The later effect is explained as generation of acceptor like states in proportion to the fluence. Thus the fluence dependence can be summarised by the following formula.

$$N_{eff}(\Phi) = N_{D,0} \exp(-c_D \Phi) - N_{A,0} - b_A \Phi \tag{33}$$

with $N_{D,0}$, $N_{A,0}$ being the initial phosphorus and boron concentrations respectively, c_D is the removal rate, b_A the generation rate of the acceptor-like states and Φ the fluence. The term b_A has been found to be equal for n-type and p-type silicon. Several experiments measured the values for c_D and b_A; $c_D \approx 2.5 \cdot 10^{-13}$ cm^2 and $b_A \approx 0.06$ cm^{-1}.

The fact that effectively n-type silicon becomes p-type under bias, has a major impact on detector-type choice. Since for the p^+n detectors the SCR after irradiation will start

**The value decreases with temperature

to grow from rear side of the detector, such a detector has to be operated fully depleted. On the other side, n^+n detector, will become n^+p detector after irradiation and it will be possible to operate it partially depleted. This may be an important fact, since the time dependence of the depletion voltage for an irradiated detector is so far not fully understood. The time dependence is shown in figure 13. The obvious difference of the

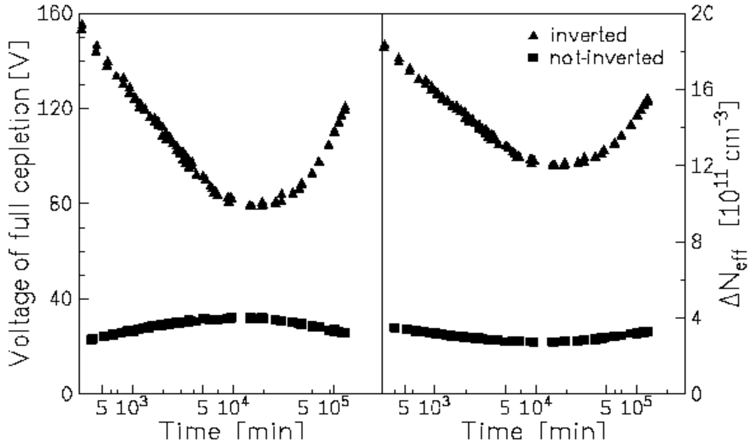

Figure 13: Left: Voltage for full depletion as function of time, right: ΔN_{eff} as function of time, for inverted and non-inverted detector.

time behaviour can be interpreted consistently by defining a quantity ΔN_{eff}

$$\Delta N_{eff}(\Phi, t, T) = N_{eff,0} - N_{eff}(\Phi, t, T) \tag{34}$$

which is the difference of the effective doping concentration before irradiation and its actual value at time t after irradiation with fluence Φ. As can be seen from the figure the effective doping concentration at first decreases, showing an annealing of defects. Then rises again exhibiting reverse annealing.

If the annealing is interpreted as a reduction of space charge the reverse annealing has to be regarded as space charge generation. It was found that data are in agreement with a second order process ($X_1 + X_2 \to Y$). Electrically inactive defects X were created by radiation damage. In time these combine to electrically active defects Y. If both X_1 and X_2 are present in similar concentrations $N_{X_1} \approx N_{X_2} \equiv N_X$ one gets

$$N_{X,0} \ = \ N_{Y,\infty} \ = \ N_X(t) + N_Y(t) \tag{35}$$

where $N_{X,0}$ is N_X at $t = 0$ and $N_{Y,\infty}$ is N_Y at $t = \infty$ and thus

$$N_Y \ = \ N_X(t = 0) - N_X(t) \tag{36}$$

The density of active defects N_Y at time t is given by (equation (30))

$$N_Y(t) \ = \ N_{X,0}\Big(1 - \frac{1}{1 + N_{X,0}\tilde{k}t}\Big) = N_{Y,\infty}\Big(1 - \frac{1}{1 + \frac{t}{t_{1/2}}}\Big) \tag{37}$$

<table>
<tr><td colspan="4">Generation : $X + X \to Y$
Basic equation: $\Delta N_{eff}(\Phi, t, T) = N_Y(\Phi, t, T) + N_C(\Phi)$</td></tr>
<tr><td colspan="4">N_C concentration of electrically active defects constant in time:
$\Delta N_C(\Phi) = N_{C,0}(1 - \exp(-c_C\Phi)) + b_C\Phi \approx$
$\approx N_{C,0} + b_C\Phi$ (for $\Phi > 10^{13}$ cm^{-2})</td></tr>
<tr><td>neutrons
protons</td><td>$N_{C,0} = 0.6 - 3.3 \cdot 10^{11}$ cm^{-3}
$N_{C,0} = 4 - 7 \cdot 10^{11}$ cm^{-3}</td><td>$b_C = 0.018$ cm^{-1}
$b_C = 0.012$ cm^{-1}</td><td>$c_C = 3.6 \cdot 10^{-13}$ cm^2</td></tr>
<tr><td colspan="4">N_X concentration of electrically inactive defects
N_Y concentration of electrically inactive defects</td></tr>
<tr><td colspan="2">$N_Y(t) = N_{Y,\infty}(1 - (1 + \frac{t}{t_{1/2}})^{-1})$</td><td colspan="2">$N_{Y,\infty} = b_Y\Phi$
$b_Y = 0.046 \pm 0.016$ cm^{-1} (neutrons)
$b_Y = 0.058 \pm 0.014$ cm^{-1} (protons)
$t_{1/2} = (N_{Y,\infty}\tilde{k})^{-1}$
$\tilde{k} = 294$ cm^3 s^{-1}</td></tr>
</table>

Table 3: Summary of second order model.

where $t_{1/2} = (\tilde{k}N_{Y,\infty})^{-1}$ is the half-life time for reverse annealing and $N_{Y,\infty} = b_Y\Phi$. The number of active defects grows linearly with fluence. Using (37) ΔN_{eff} can be written as a sum of two components N_C and N_Y:

$$\Delta N_{eff}(t) = N_Y(t) + N_C = N_{Y,\infty}\Big(1 - \frac{1}{1 + \frac{t}{t_{1/2}}}\Big) + N_C \tag{38}$$

where N_C represents all electrically active defects which remain constant in time. A set of three parameters $N_{X,0}(= N_{Y,\mathrm{inf}})$, $\tilde{k}$ and N_C are determined from fits 5.1. It has been observed N_C grows linearly with fluence as well, although exhibits slightly different behaviour at lower fluences (table 5.1). The reverse annealing has been modelled using the assumption that two different defects X_1 and X_2 of similar concentrations combine to Y. But it is rather unlikely to assume similar generation rates for X_1 and X_2, as necessary to explain that the amplitude of the reverse annealing grows in proportion to the fluence. A suitable reaction is $X + X \to Y$.

Reverse annealing can be suppressed by reducing the temperature of the detector below 5°C.

In order to find a parametrisation of short term annealing ($t < 1.5 \cdot 10^5$ min) it is necessary to subtract all long term components (reverse annealing). After subtraction one gets the concentration of annealing defects N_{ann}:

$$N_{ann}(t) \ = \ \Delta N_{eff}(t) - N_C - N_Y(t) \tag{39}$$

Usually the data are fitted to a sum of two or more exponential functions. Each exponential function can be understood as the decay of one defect.

$$\frac{N_{ann}(t)}{\Phi} = B_1 \exp(-\frac{t}{\tau_1}) + B_2 \exp(-\frac{t}{\tau_2}) \quad \Rightarrow \tag{40}$$

$$\Rightarrow \quad \Delta N_{eff}(t) = B_1 \exp(-\frac{t}{\tau_1}) \cdot \Phi + B_2 \exp(-\frac{t}{\tau_2}) \cdot \Phi + N_C + N_Y(t)$$

Typical values of time constants at room temperature are $\tau_1 \sim 2 \cdot 10^3$ min and $\tau_2 \sim 2 \cdot 10^4$ min.

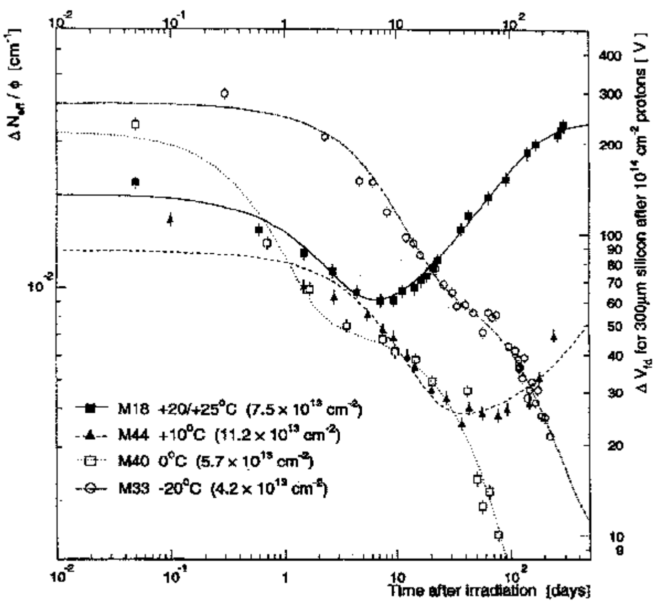

Figure 14: Evolution of N_{eff} and V_{fd} normalised to 24 GeV/c proton fluence as a function of time after irradiation for detectors kept at the temperature and fluence indicated.

5.2 Changes in Leakage Current Behaviour

The main reasons for a increase of the reverse current are recombination and generation processes (11). The generation process consists of hole emission from the trap level to the valence band and subsequent emission of an electron to the conduction band. The number of electrons which are generated per unit time $(1/\tau_g)$ by a defect-level can be calculated from its occupation probability f_T and its emission rate e_n

$$\frac{1}{\tau_g} = e_n \cdot f_T = \frac{e_n e_p}{e_n + e_p} \quad . \tag{41}$$

The bottle neck of continuous generation is always the smaller generation rate either e_n or e_p. It is evident that the generation rate $1/\tau_g$ reaches a maximum value if $e_n \approx e_p$ and this in turn requires $E_T \approx E_i$ as can be seen if (41) is rewritten (see (16))

$$\frac{1}{\tau_g} = \frac{\sigma_n\,\sigma_p\,v_n\,v_p\,n_i}{\sigma_n\,v_n\exp(\frac{E_i-E_T}{k_BT}) + \sigma_p\,v_p\exp(\frac{E_T-E_i}{k_BT})} \quad . \tag{42}$$

If $E_T = E_i$ the denominator is independent of energy level and τ_g can be simplified to

$$\frac{1}{\tau_g} = \frac{n_i}{(\sigma_n\,v_n)^{-1} + (\sigma_p\,v_p)^{-1}} \quad . \tag{43}$$

In any case for the bulk generation current it follows

$$I_{BGC} = \frac{e_o\,N_T\,A\,d}{\tau_g} \tag{44}$$

Combining the equations (43, 42) and taking into account $v_{thermal} \propto \sqrt{T}$ the temperature dependence of the generation current can expressed as follows.

$$I_{BGC} \propto T^2\exp(\frac{E_g}{2k_BT}) \tag{45}$$

It is evident, that the bulk generation current can be reduced significantly by just lowering the temperature. If instead of at room temperature the detector is operated at 10° C the current is reduced by about 70 %.

From (44) it follows that current dependence on generation centres is linear. Since radiation induces generation centres in proportion to the fluence the current depends on fluence (Φ) in the same way

$$\frac{\Delta I}{V} = \Delta J = \alpha\Phi \quad . \tag{46}$$

The change in reverse current before and after irradiation is denoted by ΔI and detector volume by V. The proportion factor is called the current damage constant, which is found to be between $5 \cdot 10^{17}$ A cm^{-1} and $10 \cdot 10^{17}$ A cm^{-1} at room temperature immediately after irradiation.

Afterwards, the time evolution of α and hence the current can be parametrised using (figure 15)

$$\alpha(t) = A_1\exp(-\frac{t}{\tau_I}) + A_2\exp(-\frac{t}{\tau_{II}}) + \alpha_\infty \tag{47}$$

After a very long time $t \geq 2 \cdot 10^5$ min the value for α i.e reverse current reaches its final value (table 4). No reverse annealing of the reverse current has been observed.

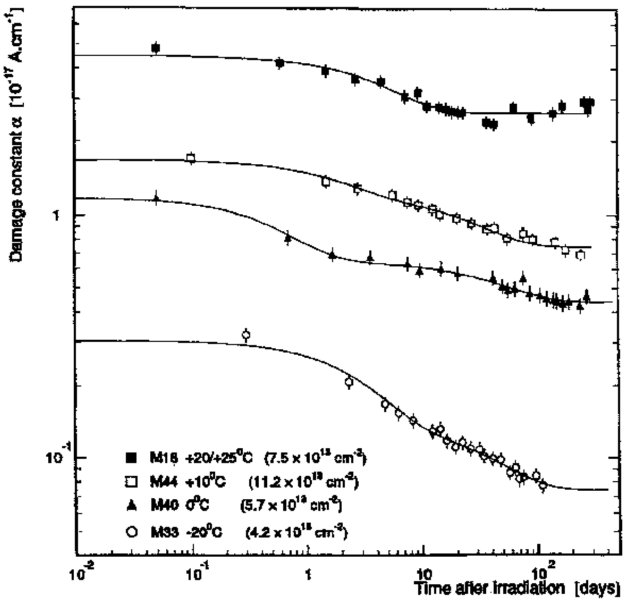

Figure 15: Leakage current damage coefficient α as a function of time after irradiation with 24 GeV/c for detectors kept at the temperature and fluence indicated.

$\tau_1 \approx 3 \cdot 10^3$ min	$\tau_2 \approx 3 \cdot 10^4$ min
$\alpha_\infty \approx 4 \cdot 10^{-17}$ A cm^{-1}	

Table 4: Approximate time constants and stable current damage constant α_∞ obtained by measuring current annealing at room temperature.

Since the amount of defects generated per fluence can be regarded as independent of the temperature, the value of α_∞ normalised to room temperature is independent of temperature as well.

Values for α measured at different temperatures are normalised to room temperature using equation (45).

If α_∞'s are plotted as a function of the reciprocal temperature (figure 15) the dependence can be represented by $\alpha_\infty = A + \exp(-B(1000/T)$. The reverse current is proportional to the carrier density n_i as ††

$$I_{BGC} \propto n_i \propto \exp(-\frac{E_g}{2k_BT}),$$

where E is the energy band gap. Using the value of B one gets $E = 1.06$ eV, which is in reasonable agreement with the half value of the silicon band gap. Thus the reverse

††Term T^2 in (45) is negligible compared to exponential term.

current at various temperatures after long term annealing is consistent with equation (45). Therefore it is concluded that the stable radiation induced damage causing the observed rise in leakage current is independent of the irradiation temperature.

5.3 Comparison of Current and N_{eff} Results

Both reverse current and effective doping concentration increase linearly with Φ after type inversion. Below type inversion N_{eff} is governed by donor removal, while current increases indeed in proportion with the fluence. The behaviour of both quantities can be comparable only in the time range below $t \approx 5 \cdot 10^4$ min, where the values of both time constants are comparable. However, by comparing both quantities it is possible to get the emission rate for the corresponding defect level.

$$I_{BGC} = e_0 \, A \, D \, N_T \, f_T \, e_n = e_0 \, A \, D \, N_{SC} \, e_n \tag{48}$$

where $N_{SC} = N_T f_T$ denotes the concentration of occupied centres contributing to the effective space charge. From here it follows

$$N_{SC} = \frac{I_{BGC}}{e_0 A D e_n} = \frac{J}{e_0 \, e_n} \quad \text{and} \quad e_n = \frac{J}{e_0 N_{SC}} \quad . \tag{49}$$

It can be seen that the contribution of generation centres to the effective space charge is governed by the emission rate. For a given current a small rate results in a stronger contribution and vice versa a large rate will result in a lower contribution. The density of reverse current J and N_{SC} can be replaced with each term corresponding the defect-level in (47) and (40), separately. The resulting emission rates are:

$$e_{n,2} = \frac{A_1}{B_1 e_0} \quad , \quad e_{n,2} = \frac{A_2}{B_2 e_0} \quad . \tag{50}$$

Very different from short term annealing is the long term annealing, because current and space charge undergo different developments. The current is found to remain constant in time, while the effective doping concentration increases again. Thus it can be definitely excluded that the defects generated during reverse annealing are correlated to the current.

5.4 Deep Level Theory

So far nothing has been said about a microscopic picture explaining the leakage current and effective doping concentration behaviour. Even if the parametrisation (33) seems to be correct, the theory of donor removal and acceptor generation appears to be insufficient, because the measured donor removal rate is by an order of magnitude too small. Lately a new theory has been proposed. A model which includes a single acceptor ‡‡ in the

‡‡Of course the model does not require that only a single deep level be present.

Poisson equation has been successfully used to describe the observed evolution of N_{eff} with neutron fluence for both p and n type detectors. This model has only one free parameter, the generation rate g_{dla} for the deep level acceptor (figure 16). Further understanding

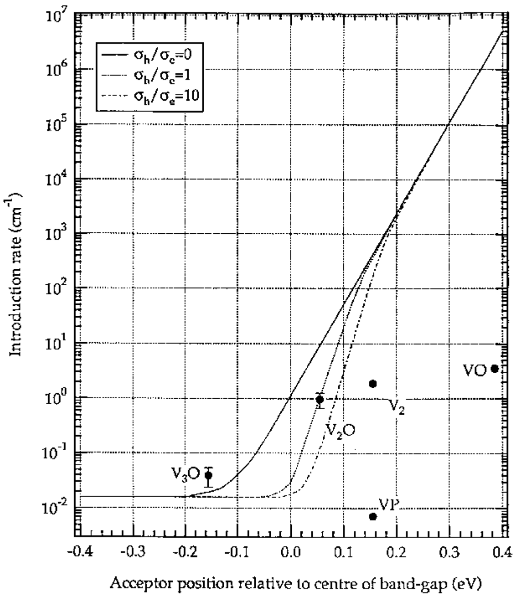

Figure 16: The introduction rate for a deep level acceptor required to be consistent with a rate of change N_{eff} = 0.016 cm^{-1}, as a function of the acceptor level within the band gap. Different assumptions for the ratio of hole and electron capture cross-sections (σ_h/σ_e) have been used; the most likely case is (σ_h/σ_e)=1. The identified candidates for such a state are plotted in the figure.

can be achieved by numerical calculations of the evolution of complex defects formed during irradiation particularly the reactions of vacancies and interstitials with oxygen and carbon. Because of its concentration ($N_O \sim 10^{16}$cm^{-3}) and capture radius, oxygen is the dominant capture site for vacancies; carbon ($N_C \approx N_O$) behaves similarly as a sink for interstitials. The effectiveness of vacancy capture at oxygen and related defects prevents significant VP ($N_P \sim 10^{12}$cm^{-3}) production despite the relatively large capture radius of phosphorus. The model supports the experimentally measured low phosphorus removal rate. The strongest candidate for such a deep level is the V$_2$0 centre.

The model should also explain the annealing behaviour of the detectors. By taking a look at equation (49), it can be concluded that the fraction of occupied levels increases with higher leakage current. For detectors irradiated past type inversion, a simple expression between deep acceptor concentration and current damage constant has been derived.

$$\frac{N_{eff}}{\Phi} \approx constant \times \sqrt{\frac{N_{SC}}{\Phi}(\frac{\alpha}{n_i})} \tag{51}$$

where N_{SC} is the concentration of filled deep acceptors. Only a small fraction f_T of deep acceptors are filled. Higher leakage currents result in more acceptors being filled which increases N_{eff}. In early phase after irradiation, the density of deep acceptors is approximately constant but fewer remain filled as the leakage current reduces during annealing.

Effective doping concentration N_{eff} starts to exhibit reverse annealing at room temperature once the leakage current reduction has ceased. This implies that N_{SC} is increasing. It has been found out that the V_3 defect disappears slowly at room temperature. At the same time the DLTS (Deep Level Transient Spectroscopy) concentration measurements show an increase of VO with the same rate as the amount of V_3 defect decreases. This must be a consequence of vacancy release and capture by oxygen. This new source of vacancies then generates more deep acceptors which causes N_{eff} to increase. This successfully explains the observed features of reverse annealing, namely the strong temperature dependence and eventual saturation of N_{eff}. The identification of the V_2O centre as the most likely candidate for the deep acceptor is also consistent with this picture; the "delayed" vacancies react with VO to form more V_2O defects.

$$\mathrm{V + O \rightarrow VO + V\ (delayed) \rightarrow V_2O \quad \equiv \quad V + V + O \Longrightarrow V_2O}$$
$$(\text{since } N_O \sim 10^{16}\text{cm}^{-3} \gg N_V \text{ - second order process})$$

The origin of a significant V_3 concentration can be explained only by production in PKA cascades (cluster formation) during the irradiation. This is consistent with enhanced V_2 production observed in neutron irradiation and is expected from the defect reaction picture where mobile vacancies combine with each other and static V_2 in the cluster volume. Since the cluster is a region of volume $(\sim 10\text{nm})^3$ only 0.01 oxygen atom on average corresponds to a cluster. Therefore it is obvious why V_2O and V_3O are formed instead of VO. That also explains why reverse annealing of effective doping concentration was not observed by photon and electron irradiation, where clusters are not formed.

If the deep energy level model is generally correct, key ingredients in possible radiation harder detectors may be oxygen and carbon since these are the dominant capture sites for vacancies and interstitials. High oxygen concentration suppresses phosphorus removal and encourages VO centre formation in expense of V_2O and V_3O. The VO centre is relatively harmless because on its distance in energy from mid-gap, so an increase in in the initial oxygen concentration may be beneficial. In case of carbon it appears that either a significant increase or decrease in concentration may be beneficial. If carbon concentration is reduced, the accumulation of multi-vacancy complexes is reduced by the availability of more interstitials for recombination. Conversely, modelling suggests that higher carbon concentration can reduce the free vacancy population because of the importance of the reaction $\mathrm{I+V_2 \rightarrow V}$.

5.5 Charge Collection

Electrons and holes generated by particles crossing the detector drift to the electrodes due to electric field. Some of drifting charge carriers are captured by defect-levels and trapped for a while before being re-emitted again (figure 11). The probability of a charge carrier to be trapped depends on the cross section of the trap levels $\sigma_{n,p}$, the drift velocity v_D of the charge carriers and of course, on the concentration of the trap N_T. It is useful to define a trapping time constant

$$\frac{1}{\tau_T} = N_T v_D \sigma \quad , \tag{52}$$

which allows the description of the fraction of charges trapped per time by the following equation:

$$-\frac{dQ}{Q} = \frac{dt}{\tau_T} \quad . \tag{53}$$

By integrating left and right side it follows

$$\frac{Q_{irr}}{Q_0} = e^{-\tau/\tau_T} \quad (\text{typically } \frac{Q_{irr}}{Q_0} = 0.9 - 1) \tag{54}$$

where Q_{irr} denotes charge collected after irradiation, Q_0 charge collected before irradiation and τ the charge collection (shaping) time (same τ as in (6)). Trapping time constants were found to be in the order of μs depending on the fluence as $\tau_T \propto 1/\Phi$.

The optimum shaping time to be used with irradiated detectors is found to be between $\tau = 20 - 50$ ns. At higher values the noise increases because of the high leakage current (6), so that the gain in collected charge can not compensate the increase of noise and S/N drops. At lower values a large fraction of charge is lost due to short collection time, and S/N decreases as a consequence of the second term in (6) as well.

Normally one would expect the collected charge (signal) to grow as $Q \propto D \propto \sqrt{V}$, which is true for unirradiated detectors. For irradiated detectors, however, linear dependence seems to be more appropriate (figure 17). This implies that (4) does not describe $D(V)$ correctly. Beside that, the values obtained from CV measurements of full depletion voltage are smaller with the ones derived from measuring the signal. At full depletion voltage the scattering from defects reduces the carrier mobility to such extent, that it is impossible to collect all the charge. This means that the detectors should be over-depleted in order to get the highest S/N.

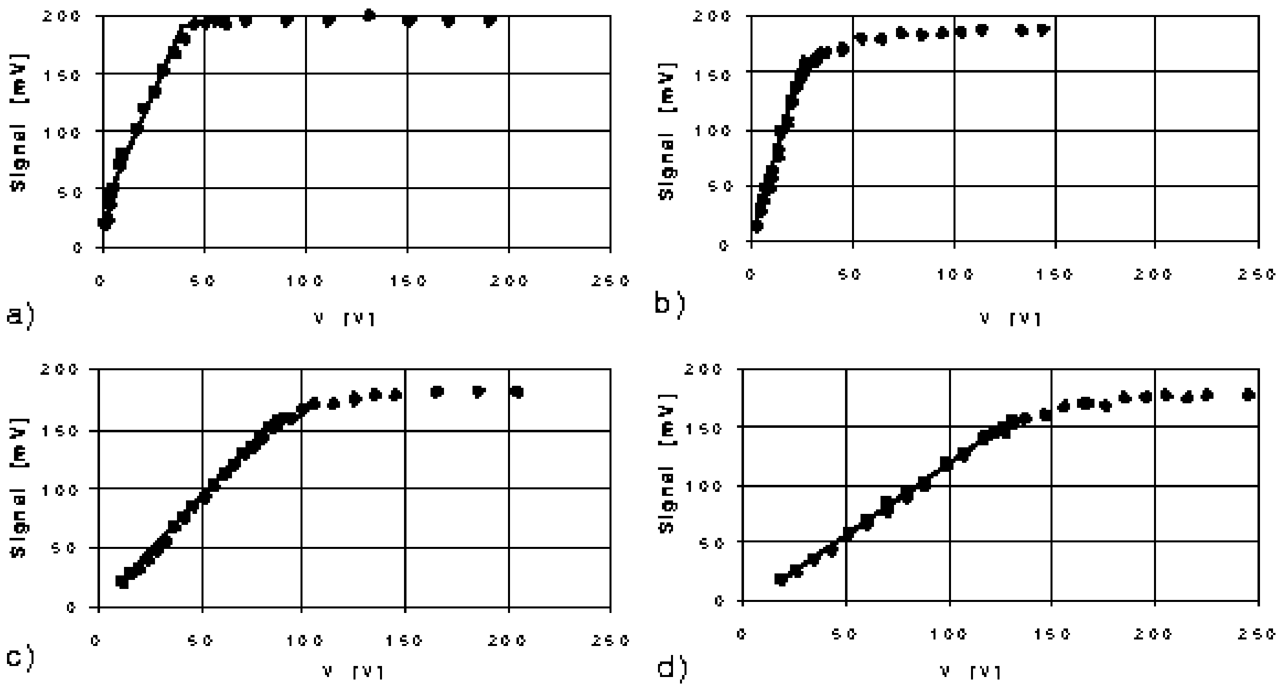

Figure 17: The signal (mV) as a function of applied voltage for a non-irradiated detector (a.) and detectors irradiated at various proton fluences: $2.8 \cdot 10^{13}$ cm^{-2} (b.), $6.2 \cdot 10^{13}$ cm^{-2} (c.), $1.2 \cdot 10^{14}$ cm^{-2}. The lines represent a fit to a function $konst \cdot V^n$ with $n = 0.58$ (a.), 0.99 (b.), 1.05 (c.), and 1.1 (d.).

References

[1] T. Schultz, *Investigation on the Long Term Behaviour of Damage Effects and Corresponding Defects in Detector Grade Silicon after Neutron Irradiation*, doctoral thesis, Universität Hamburg, 1996.

[2] F. Lemeilleur *et. al.*, *Study of Characteristics of Silicon Detectors Irradiated with 24 GeV/c Protons Between -20°C and +20°C*, CERN Preprint (CERN-ECP/94-8), 1994.

[3] G.Hall , *Radiation Damage to Semiconductors*, Conference Proceedings Vol.46, SIF, Bologna, 1994.

[4] G. Hall , *Radiation Damage to Silicon Detectors: Past and Future*, Preprint IC/HEP/96-1, Presented at the International Conference on Radiation Effects on Semiconductor Materials, Detectors and Devices, Florence, 1996.

[5] J. Matheson *et. al.*, *A Microscopic Explanation for Type Inversion and the Annealing Behaviour of Radiation Damaged Silicon Detectors*, Preprint (IC/HEP/95-4), 1995.

[6] RD2 Collaboration, *Pion-Induced Damage in Silicon Detectors*, CERN Preprint CERN-ECP/95-26, 1995.

[7] RD20 Collaboration, *Radiation Tolerance of Single-Sided Silicon Microstrips*, CERN Preprint CERN-PPE/93-137, 1993.

[8] John. A.J. Matthews *et. al.*, *Bulk Radiation Damage in Silicon Detectors and Implications for LHC Experiments.*, to be published in Nucl. Instr. and Meth. in Phys. Res. A. (Preprint NMCPP/96-01), 1996

[9] C. Leroy *et. al.*, *Study of Charge Collection and Noise in Non-Irradiated and Irradiated Silicon Detectors*, CERN Preprint CERN-ECP/96-05, Presented at the International Conference on Radiation Effects on Semiconductor Materials, Detectors and Devices, Florence, 1996.